Modelling Simul. Mater. Sci. Eng. **8** (2000) 665–676. Printed in the UK PII: S0965-0393(00)15623-2

Dynamics of clustering in a binary Lennard-Jones material

I Skauvik†‡, J P Hansen†‡ and T Matthey§

† Institute of Physics, University of Bergen, Allégaten 55, N-5007 Bergen, Norway
‡ Hydro Aluminium a.s, R&D Materials Technology, Håvik, N-4265 Karmøy, Norway
§ Department of Informatics, University of Bergen, Høyteknologisenteret i Bergen, N-5020 Bergen, Norway

Received 28 February 2000, accepted for publication 10 July 2000

Abstract. We have performed constant temperature two-dimensional molecular dynamics simulations of a binary Lennard-Jones material, representing an idealized metallic alloy or a material containing a specified fraction of an additive atomic species. Differences in the interatomic potentials between the atomic species can lead to clustering of the alloy atoms. An exponential distribution of cluster size is obtained as time approaches infinity. For sufficiently strong attractions the distribution of cluster sizes becomes nearly independent of the force and the attained maximum cluster size reaches a saturation level.

1. Introduction

Aggregation and fragmentation are fundamental processes occurring in a variety of phenomena in nature on a wide range of length and time scales [1]. A fundamental problem within irreversible aggregation is to determine the final cluster size distribution and the dynamics of the clustering process. Such processes may take place whenever a large number of particles or elements are allowed to interact for a sufficient length of time. The time scale may be from billions of years to femtoseconds or below, depending on which particular systems are being studied.

In industry irreversible segregation and aggregation processes are often unwanted side effects which need to be minimized or controlled. A particular example concerns the role of such processes in casting, heat treatment and working of metallic alloys: the segregation of alloy atoms may, for example, reduce to a significant degree the quality of the final product. Therefore, there is a quest to model these phenomena to support process control. There are, however, some serious difficulties when handling these phenomena in macroscopic models based on classical continuum mechanics. Such models generally fail in handling the formation of voids and shrinking effects which violate the simple continuum equation, $\nabla \cdot \vec{u} = 0$.

With the development of supercomputers such processes may alternatively be studied directly by molecular dynamics (MD) simulations with a large number of interacting particles. Within this approach, aggregation occurs as a phase transition from an initial unstable configuration towards a stable equilibrium configuration. Quite a few MD simulations of non-equilibrium phase transitions have been reported for a variety of phenomena and for a few recent examples we refer the reader to [2–4]. The technique has also proved to be feasible for studies of diffusion and ion transport phenomena [5, 6].

In the present paper we report MD simulations of clustering in a dense binary Lennard-Jones fluid. This model is the simplest representation of a material doped by a second atomic

0965-0393/00/050665+12$30.00

species. The paper is organized as follows. The next section presents the simulation model and discusses the basic reaction dynamics. In section 3 the simulation results are analysed and in section 4 conclusions are drawn. Unless explicitly mentioned, units of mass, energy and length are given by atomic mass units (AMU), electron volts and ångströms which gives a time unit equal to 1.02×10^{-14} s.

2. Simulation model and dynamics

The simulation is initiated by positioning bulk particles with a given radius in a close-packed, two-dimensional lattice. A certain defined fraction of the bulk particles is randomly replaced by a new particle type which constitutes an alloy particle. A constant temperature $T_c = 100$ K is simulated by assigning a random Gaussian distributed velocity to each particle. A given fraction of the particles is defined as alloy atoms. The system then evolves in time according to Newton's law,

$$m_i \frac{d^2}{dt^2}\vec{r}_i = \left(\sum_j \vec{F}_{j,i}\right) - \xi(\langle T(t)\rangle - T_c)\frac{d}{dt}\vec{r}_i. \tag{1}$$

The last term acts as a thermostat which adds (extracts) energy to (from) the system in proportion to the velocity and with the sign determined by the instantaneous value of the temperature (kinetic energy), $\langle T(t)\rangle$. The constant parameter ξ is set to 1.0 and has been found to have no influence on the simulation results for an order of magnitude range around this value. This equation is discretized and integrated in constant time steps based on the standard leap-frog [7] numerical scheme.

The two-body forces included in this model are derived from a Lennard-Jones potential,

$$V_{ij}(r_{ij}) = F_k\left(\left(\frac{r_1}{r_{ij}}\right)^{12} - \left(\frac{r_2}{r_{ij}}\right)^{6}\right) \tag{2}$$

where $r_{ij} = |\vec{r}_i - \vec{r}_j|$. More advanced metal potentials [8, 9] or other realistic types of interaction would certainly represent a better description of real metals. The simplified force calculation as well as the easy implementation of a computational grid do, however, favour the Lennard-Jones interaction, in particular, in this phenomenological study. For the bulk particles the parameters are given as $F_k = 0.3$ eV, $r_1 = 2.78$ Å and $r_2 = 3.05$ Å, as previously used in a phase equilibrium study of Ti–Al [10]. The parameters for the alloy atoms were kept constant, except for the parameter controlling the force between the reactive particles, F_k, which was varied.

In addition to the intra-species pair potentials, there is also a need to handle the interaction between the alloy atoms and the bulk atoms. In the present study we focus on the dynamics of the alloy particles, so the inter-species force is first kept equal to the force between the bulk particles. Test calculations with varying forces between the alloy and bulk particles, from purely repulsive, i.e. $r_2 = 0$, to a twice as strong force constant, $F_k = 0.6$ eV, showed that this interaction has a small influence on the general cluster distribution. At one point, however, if the inter-species force becomes strong enough, it will inhibit aggregation to some degree since the bulk particles in that situation will stick very hard to the alloy particles, and thus lower the mobility.

The general n-body problem involves $n(n-1)/2$ calculations to compute the forces for each particle, which leads to a quadratic relationship between the number of particles and the computation time. By introducing a finite interaction range, ($r_{\text{cut-off}}$), the computational amount is considerably reduced. For large systems each particle's position and its neighbours' need to be traced in some way. Instead of using a neighbour list the simulation space is divided

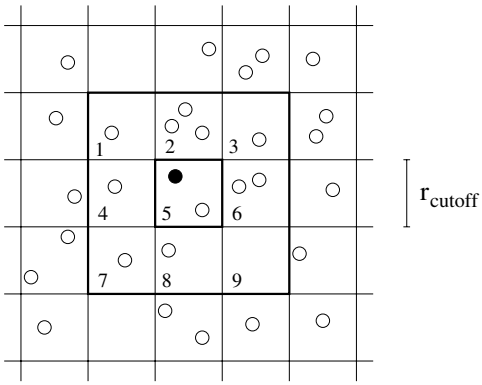

Figure 1. Partition in quadratic cells, where cell 5 is the reference and 1–4, 6–9 are the neighbouring cells.

into quadratic cells, cf figure 1, of size at least $r_{\text{cut-off}}$, as in [11]. We assign each particle to its corresponding (spatial) cell by an index/pointer. For computation of the interactions for a given particle we have to consider all other particles of the same cell and the particles of the eight adjacent cells. Thus, we achieve a linear relation between particle number and computing time.

After each computational step, the index/pointers of the particles moving from one cell to another need to be updated. In our implementation we use the path 5–6–3–2–1 [11], where cell 5 is the reference cell and 1, 2, 3 and 6 are the adjacent cells. Using Newton's third law and paying special attention to the interactions inside the reference cell, the sum of all paths covers all possible interactions with the given $r_{\text{cut-off}}$. To increase the performance we apply OpenMP [12] to parallelize the computation where each process/thread can compute the forces independently due to local spatial properties of the cell algorithm.

Figure 2 shows a snapshot of a part of an initial arrangement of a two-dimensional close-packed structure with 92 000 matrix atoms. In this example 10% of the atoms have been assigned the properties of the alloy species and are highlighted in the figure. The initial temperature was set to 100 K. Other temperatures were also simulated, but only small effects were observed in the temperature range from 10–500 K. This is explained partly by the fact that a two-dimensional system is highly constrained. Open boundary conditions were used, but test calculations with periodic boundaries showed no structural change in the final state. The breakup temperature of the sample was around 1500 K and depends slightly on alloy concentration.

The initial state is modelled by exchanging a pre-defined fraction of the matrix atoms with the alloy atoms using a random number generator. Therefore, there is a certain probability of n-atomic ($n > 1$) molecules being present initially. There will be a spontaneous formation of heavier molecules whenever the attractive forces between the constituent atoms exceed the local forces that try to maintain the close-packed matrix structure. In these simulations only the formation of heavier molecules from smaller molecules is observed, and never the opposite. Therefore, a state of chemical equilibrium is not expected to occur, but rather a state of saturation or pseudo-equilibrium. As will become clear, the non-equilibrium dynamics will depend on having enough local energy to rearrange the atomic structure. This energy is induced by a series of collisions initially from a migrating alloy particle. We are therefore unable to predict the final distribution of cluster configurations from standard thermodynamic theories of binary solutions.

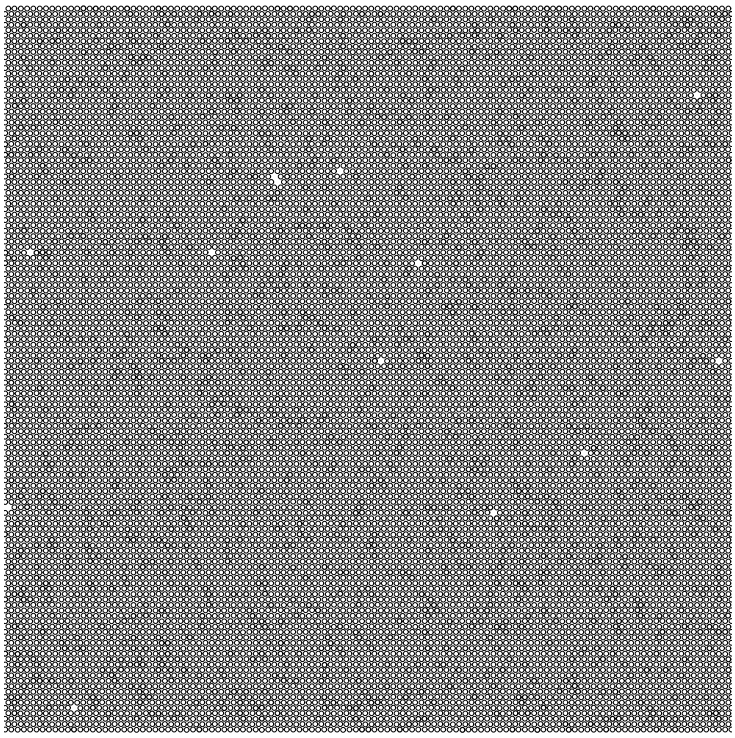

Figure 2. Sample of a part of a configuration with 92 000 particles after a few time steps. Each particle is represented by a circle and the alloy particles are highlighted.

In figure 3 the structure of figure 2 is shown in the final configuration. A range of cluster sizes and shapes can be seen. The structure of the matrix also varies from close-packed stable structures to those strained or which are completely amorphous. The void fraction has also increased and these 'nano-pores' tend to be formed around, or close to, the clusters. In the vicinity of some clusters an amorphous phase of the matrix particles is formed, very likely due to locally-induced stresses by moving reactants. The closed-packed structure is present in the clustered groups of the alloy atoms, but there the cell constant is different from the matrix cell constant. A fraction of the alloy atoms is also seen to remain in a non-clustered state.

In order to study the dynamics of the cluster formation, a smaller model has been made. This facilitates the study of the steps of cluster formation in detail. In a small system the energy release connected with the formation of a single cluster is large enough to give a significant increase of the average temperature of the system. The built-in thermostat of the model will rapidly pull down the temperature again. A plot of system temperature versus time will therefore show peaks at the times of cluster formation. Without the thermostat, the released energy would rapidly cause the system to evaporate. For a large system the temperature peaks will be elusive, but for smaller systems the peaks are conspicuous, and it is possible to identify the process steps that give rise to the energy outbursts.

Figure 4 shows an example of the temperature development with time for a small system. It should be noted that the energy outbursts occur most frequently in the beginning, but that peaks can also be observed after long periods of time at pseudo-stability. Three temperature peaks at selected time regions are indicated with arrows. These peaks result from the formation

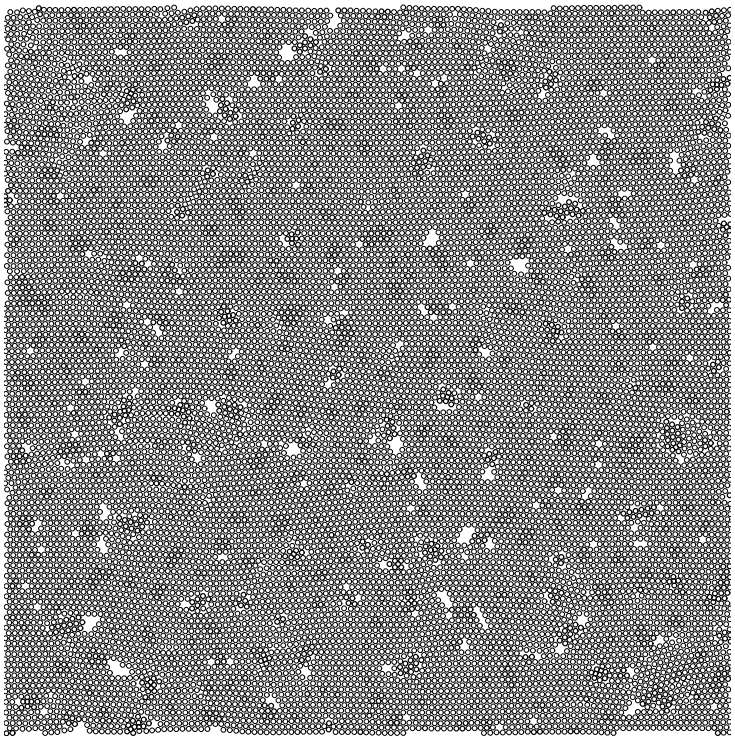

Figure 3. The same sample as shown in figure 2 at equilibrium ($T = 2.2 \times 10^{-11}$ s).

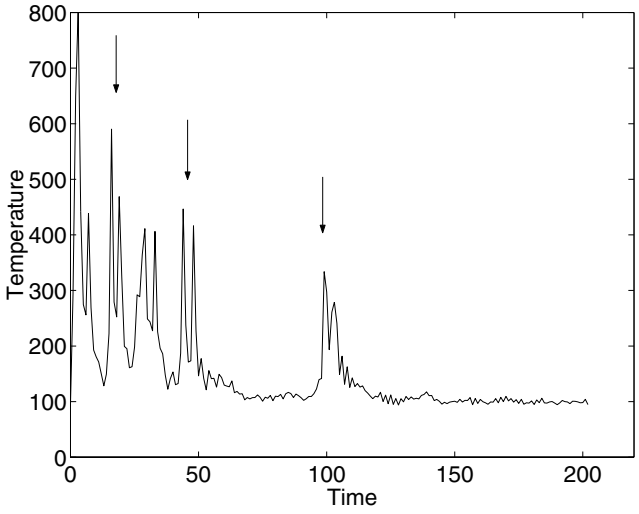

Figure 4. Temperature versus time in a model containing 900 particles, cf figure 5. The arrows indicate three aggregation events shown in figure 5.

of a specific cluster containing four atoms asymptotically. The sample is shown in figure 5. The interesting region is marked with a circle and the four clustering particles are shown as full circles. The upper panels show snapshots of the configuration before and after the first two

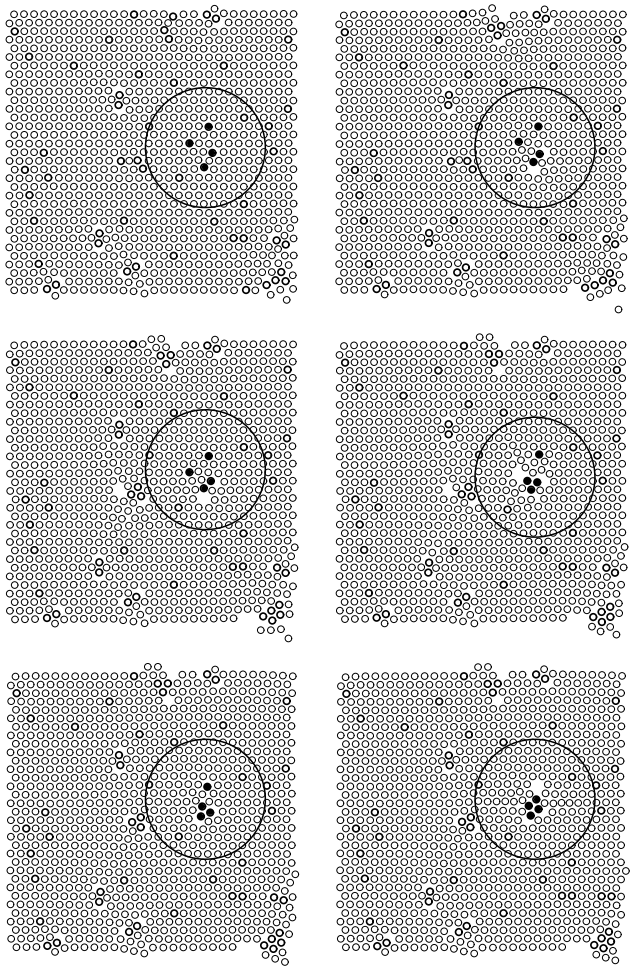

Figure 5. Snapshots of the time development of the spatial distribution of a small sample containing 900 particles. Four aggregating particles are followed and they are marked as full circles. The snapshots are taken before and after each sequence shown by arrows in figure 4. The left panels show the configuration before each transition and the right panels show the configuration after the transition.

particles have formed a diatomic molecule. The left and right panels in the middle show the configuration before and after the third particle has entered the cluster and the lowest panels show the similar situation before and after all four atoms have grouped together.

It is also illustrative to view this particular aggregation process in terms of the time development of the average interatomic distance, cf figure 6. Here the average distance between these four particles is shown as a function of time. It is interesting to note that the 'clustering times' are very short and characterized with a sharp decrease of the average distance. The clustering times are separated by much longer 'waiting times' with much lower particle velocities. An aggregating particle typically undergoes an avalanche-like motion towards a larger molecule at a point when it has enough energy to break the first barrier of the separating row of atoms. By visual monitoring of moderate-sized systems tendencies to form chain reactions can be observed. The energy release of a reaction between two atoms may

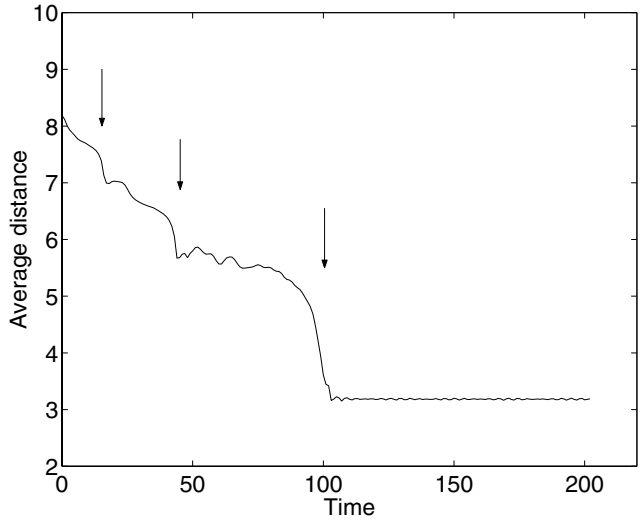

Figure 6. The time dependence of the average distance between the four particles followed in figure 5.

trigger the formation of other clusters in the neighbourhood because the increased amplitude of lattice vibrations increases the probability of two atoms exchanging their position in the structure.

3. Analysis

A quantitative characterization of the atomic arrangement is given in terms of the size distribution of the clusters. For a given initial state and a set of constants this distribution will be time dependent. The number of single atoms and small clusters will decrease with time.

Figure 7 shows examples of the size distribution at the end of the simulation interval. For all simulated cases a near exponential size distribution is observed, i.e. $\log[a_i] = k_0 + k_1 \times \log(i)$, where $[a_i]$ denotes the concentration of i-atomic clusters. The magnitude of the negative constant k_1 depends on the force constant and the initial concentration of the alloy atoms. At very low concentrations the uncertainty of the size distribution becomes elusive due to the fact that only a few clusters are present in the simulated sample, and thus the statistics become poor.

Analysis of these results shows that there is a threshold value of the constants at which clustering sets on. When the force constant between alloy particles is only slightly larger than the force between the bulk atoms, the bulk particles effectively block the alloy particles' ability to move. For extremely large force constants between the alloy particles the maximum cluster size formed is independent of the force constant. This is readily seen if the maximum cluster size (or the magnitude of k_1) is plotted versus the force constant F_k, cf figure 8.

The saturation in maximal cluster size is related to the short-range nature of the two-body forces. For N particles to coalesce into one cluster, the asymptotic force from $(N-1)$ atoms assumed to be clustered has to exceed the critical magnitude, F_c, for the last atom to move,

$$\frac{(N-1)F_k\alpha}{r_N^7} > F_c \Rightarrow r_N < \left(\frac{(N-1)F_k\alpha}{F_c}\right)^{1/7}. \tag{3}$$

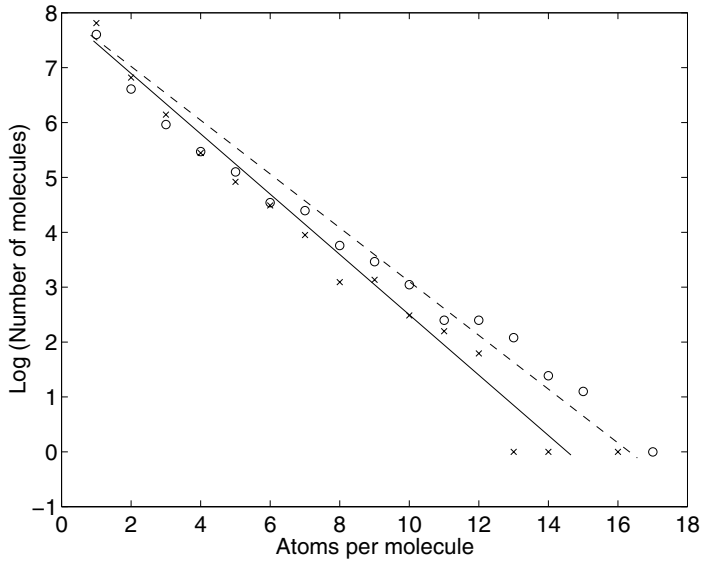

Figure 7. Cluster size distributions for two different force constants between the alloy particles; crosses, $F_k = 8$ eV; circles, $F_k = 20$ eV. The straight lines are linear fits to the simulation results. The size distribution is simulated at the end of the computation interval.

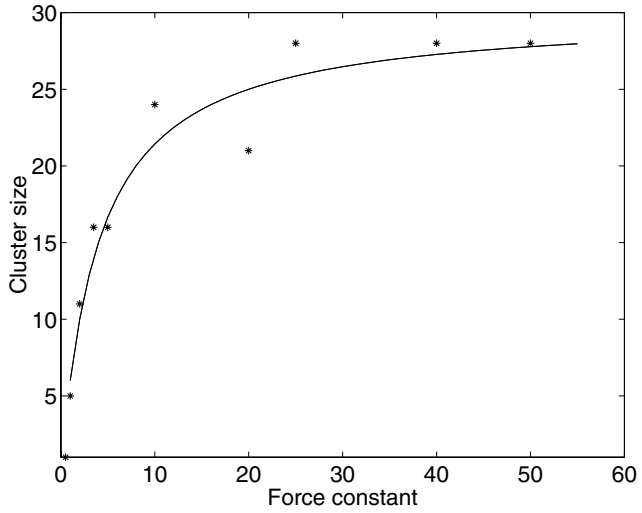

Figure 8. Number of atoms in the largest cluster as a function of the force constant F_k, cf equation (2), between the reactive particles for a 10% alloy density. The stars show simulation results, and the full curve is a fitted function.

Thus r_N increases very slowly with both N and F_k. The probability of having N alloy particles initially present inside a disc with radius r_N will, on the other hand, decay fast for large N and at some point the probability for fulfilment of equation (3) vanishes.

The ability that the single atoms have to react depends on their relative distance. For a given concentration of the alloy particles there will be an expected distribution of the distances

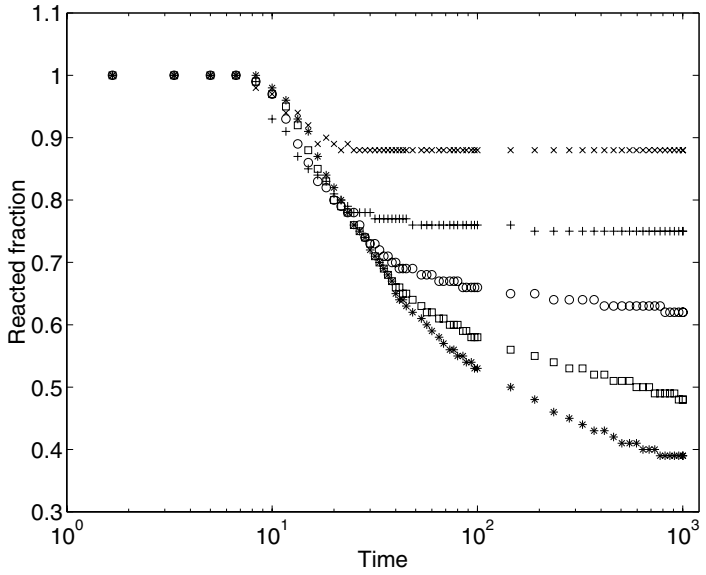

Figure 9. The unreacted fraction of single alloy atoms for five different cases with different initial concentrations of the alloy species. The concentrations are 2% (×), 5% (+), 8% (○), 10% (□), 14% (*). All curves are scaled with respect to the number of single atoms at the initiation of the simulations. This number is smaller than the total number of alloy atoms due to the fact that some clusters are present initially.

between these atoms. When there is a low concentration of alloy atoms, there will be a high fraction of atoms where the distance to the nearest neighbour is too large for the formation of clusters. Such atoms can be denoted as 'non-reactive alloy atoms' (NRAA). They are locked in the close-packed matrix structure, and are expected to stay within the matrix corresponding to a solid solution state. The fraction of NRAA will drop as the initial concentration increases. Therefore, a larger fraction of the initial atoms will form clusters when the concentration of the alloy atoms is higher. This is clearly seen from the simulation results shown in figure 9 where the unreacted fraction of single alloy atoms is plotted versus time for different initial concentrations.

For a low concentration alloy (2%), slightly above 10% of the single constituent atoms react, and saturation is reached within a short period of time. Figure 9 shows that there is a near linear relationship between the initial concentration and the reacted fraction. Some allowance most be made for the fact that the saturation state is not reached for the higher concentrations. The initial concentration used for a reference in figure 9 is the initial concentration of single alloy atoms. This is not necessarily equal to the total alloy concentration, since some of the additive may initially be present as diatomic and larger clusters. One conspicuous feature of the graphs in figure 9 is the initial time interval when no reaction takes place. The explanation is simply the fact that some time is needed to transport a non-clustered atom to a position in the cluster.

The gross features of the clustering dynamics may be modelled based on the theory of irreversible aggregation [14]. The assumptions that only binary collisions between n-atomic and m-atomic cluster sizes occur and that such a collision leads to a $(n + m)$-sized atomic cluster with a collision rate $K_{n,m}$ leads to the kinetic rate equations for the number of k-sized

clusters N_k,

$$\frac{\mathrm{d}N_k}{\mathrm{d}t} = \frac{1}{2}\sum_{i=1}^{k-1} K_{i,k-i}N_i,\, N_{k-i} - N_k \sum_{i=1}^{N_{\max}} K_{i,k}N_i. \tag{4}$$

For finite $N_{\max}$, this system may be solved numerically with initial conditions $[N_1(t_0), N_2(t_0), \ldots, N_{\max}(t_0)] = [N_1, 0, \ldots, 0]$. An extensive literature [13] exists on analytical solutions of these equations, which depend very strongly on the structure of the collision rates. In particular, for matrices which scale with the indices as

$$K_{ai,aj} = a^{\lambda} i^{\mu} j^{\nu} \tag{5}$$

several analytic properties are known. The best known case is when all matrix elements are equal, i.e. $\lambda = 1$, $\mu = \nu = 0$. In this case the solution of equation (3) is given by [14]

$$N_k(t) = \frac{N(\frac{1}{2}aNt)^{k-1}}{(1 + \frac{1}{2}KNt)^{k+1}} \tag{6}$$

which shows that all atoms coalesce into one large N-atomic cluster as $t \to \infty$. For other scaling properties it has been shown that a exponential tail of the cluster distribution is asymptotically obtained [15], i.e.

$$N_k(t) = c_1 k^{c_2}\, \mathrm{e}^{-c_3 k} \tag{7}$$

with c_i some positive constants. This is the same asymptotic solution as obtained in the present simulations.

In a situation when the reactive atoms are embedded in a material, a different form of the reactance matrix, $K_{i,j}$, is suggested. It is first noted that the avalanche-like motion of the single atoms separated by long stationary waiting times suggests that single atoms constitute the most active movers, i.e. $K_{i,j} = a_i(\delta_{i,1} + \delta_{1,j})$ to a first approximation. The constant a_i is essentially the probability for a single particle to be located inside the reaction area of a pre-existing $(i-1)$-sized molecule, cf equation (3). We therefore suggest a scaling function similar to equation (5), $a_i = a_0 i^{2/7}$, which identifies the aggregation rate constants with an effective reaction area. To model the time-dependent isolation of the NRAA atoms we introduce an effective number N_1^* of reacting single atoms as

$$N_1^* = N_1 \tan^{-1}\left(\alpha\left(\frac{N}{N_1(t_0)} - \beta\right) + \frac{\pi}{2}\right). \tag{8}$$

Here $N = \sum_k N_k(t)$ is the total number of particles and α, β are two free parameters controlling the transition from $N_1^*(t_0) = N_1(t_0)$ to $N_1^*(t) = 0$ for $t \to \infty$. In figure 10 the cluster size distributions following on from these rate equations with $\alpha = 5000$ and $\beta = 0.5$ are compared with MD simulations. In the upper panel, the scaling constant is taken directly from equation (3), i.e. $a_i = a_0 i^{2/7}$. In the middle panel the scaling constant is doubled allowing for an increased mobility around large clusters, since the matrix atoms may contain areas of locally melted regions, cf figure 3. The lowest panel shows the cluster size distribution from the MD simulation with $F_k = 25$ eV. A good agreement between the aggregation theory and the MD simulations is obtained with respect to the cluster size distribution. The MD simulations do, however, show a tendency to form larger clusters than the aggregation results. The overall similarity between the distributions allows us to conclude that the present aggregation model captures the essential dynamics of the MD simulations: single particle motion towards an exponential cluster size distribution and a concentration-dependent fraction of atoms which is prevented from reacting.

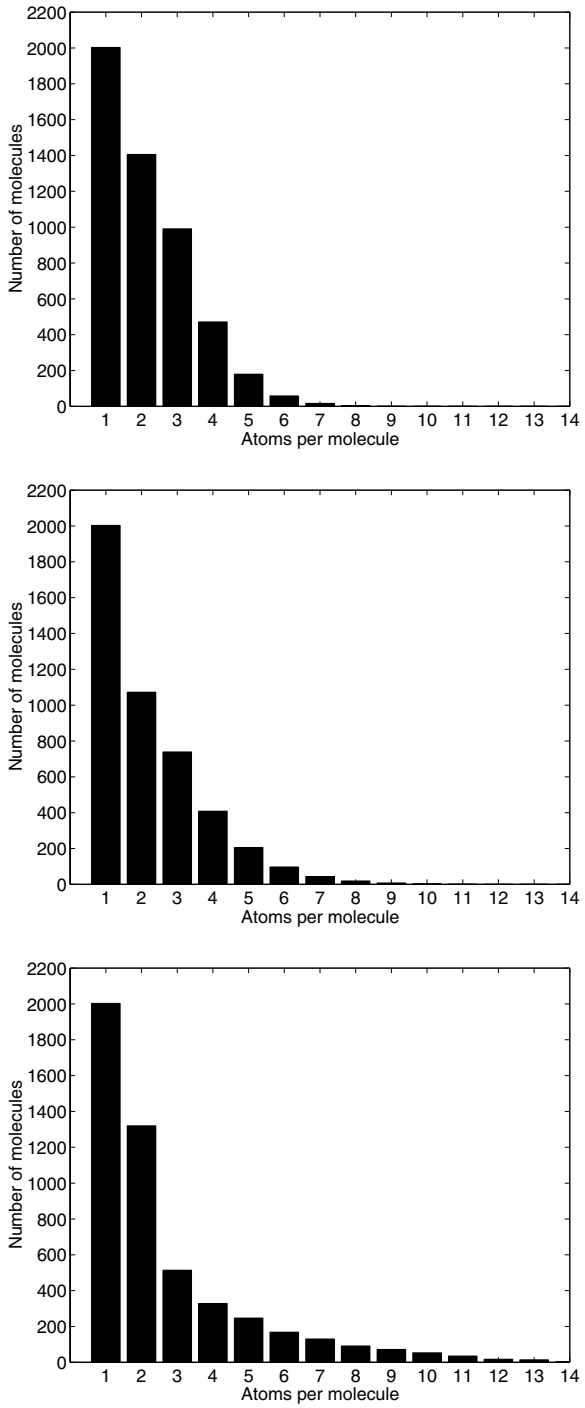

Figure 10. Cluster size distributions at $t \rightarrow \infty$ for the modified aggregation theory (upper and middle) and the MD simulations (bottom) (with $F_k = 25$ eV). In the upper figure the reactance matrix scales with an exponent equal to $2/7$, whereas the middle figure has a scaling exponent equal to $4/7$. The number distribution of the aggregation theory is normalized to the number of non-reacting particles of the MD simulations.

4. Conclusion

In the present paper we have reported results from a series of two-dimensional MD simulations of 92 000 particles consisting of bulk-type, aluminium-like Lennard-Jones particles and a small fraction of strongly interacting alloy particles. The simulations have shown that nanoscale clustering in a initially dense material is strongly sensitive to the strength and range of the attraction of the alloy particles with reference to the binding forces between the bulk particles. Clustering only starts as the force between the reactive particles exceeds a threshold value. This value depends on the activation energy for atomic rearrangement in the close-packed matrix structure.

The dynamics of the clustering is characterized by a short density-independent initialization period followed by a long clustering period which increases with alloy density. During the aggregation period only a certain fraction of the smallest molecules move. The single particle motion is characterized by fast rearrangements and long periods without significant mobility. The cluster size distribution has been found to be exponential and nearly independent of the interaction force between the alloy particles in the strong attraction regime. A modified aggregation model based only on single particle motion has verified a cluster size distribution in good agreement with the MD simulations.

Acknowledgments

This research has been sponsored by Norges Forskningsråd through a grant from 'Mobilitetsprogrammet'. The calculations were performed at the Norwegian super-computing facilities through a TRU grant.

References

[1] Shmelzer J, Röpke G and Mahnke R 1998 *Aggregation Phenomena in Complex Systems* (Weinheim: Wiley–VCH)
[2] Toxvaerd S 1998 *Phys. Rev.* E **58** 704
[3] Hirsfield D and Rapaport D C 1997 *Phys. Rev.* E **56** 2012
[4] Johnson G, Mel'cuk A I, Gould H, Klein W and Mountain R D 1998 *Phys. Rev.* E **57** 5707
[5] Hafskjold B and Li X 1995 *J. Phys.: Condens. Matter* **7** 2949
[6] Derlet P M, Høyer R, Holmestad R, Martinsen K and Ryan N 1999 *J. Phys.: Condens. Matter* **11** 3663
[7] Allen M P and Tildesley D J 1987 *Computer Simulation of Liquids* (Oxford: Clarendon)
[8] Daw M S and Baskes M I 1984 *Phys. Rev.* B **29** 6443
[9] Stolze P 1994 *J. Phys.: Condens. Matter* **6** 9495
[10] Onodera H, Nakazawa S, Ohno K, Yamagata T and M 1991 *ISIJ Int.* **31** 875
[11] Beazley D M and Lomdahl P S 1993 *Message-Passing Multi-Cell Molecular Dynamics on the Connection Machine 5* Theoretical Division and Advanced Computing Laboratory, Los Alamos National Laboratory, Las Alamos, New Mexico 87545
[12] 1997 OpenMP: A proposed industry standard API for shared memory programming *Technical Report* http://www.openmp.org, October
[13] See e.g. van Dongen P G J and Ernst M H 1985 *J. Phys. A: Math. Gen.* **18** 2779
Botet R and Jullien R 1984 *J. Phys. A: Math. Gen.* **17** 2517
Costas M E, Moreau M and Vicente L 1995 *J. Phys. A: Math. Gen.* **28** 2981
[14] Smoluchowski M V 1916 *Z. Phys.* **17** 557
[15] Villarica M, Casey M J, Goodisman J and Chaiken J 1993 *J. Chem. Phys.* **98** 4610